Research article

Linear manipulator: Motion control of an *n*-link robotic arm mounted on a mobile slider

Sandeep Ameet Kumar [a,*], Ravinesh Chand [a,b], Ronal Pranil Chand [b], Bibhya Sharma [a]

[a] *School of Information Technology, Engineering, Mathematics & Physics, The University of the South Pacific, Fiji*
[b] *School of Mathematical & Computing Sciences, Fiji National University, Fiji*

ARTICLE INFO

ABSTRACT

Linear manipulators are versatile linear robotics systems that can be reprogrammed to accommodate product changes quickly and are flexible to meet unique requirements. Such robotic systems tend to have higher accuracy, making them the perfect automation solution for those mundane, repetitive tasks. With the demand for linear systems in real-life applications expanding consistently, this paper addresses motion planning and control (MPC) of a new modified unanchored linear manipulator consisting of an *n*-link robotic arm mounted on a mobile slider along a rail. Using the method of the Lyapunov-based Control Scheme (LbCS), new centralized acceleration-based controllers are designed for the navigation of the system to an unreachable target. Via the scheme, the unanchored manipulator can perform assigned tasks with enhanced reachability. The limitations and singularities of the linear manipulator are treated as artificial obstacles in this motion control scheme. The robotic arm manipulator utilized in this research can reposition its base link to a desired location in the workplace due to changes in work requirements. The effectiveness of the motion planner and the resulting acceleration-based control laws are validated numerically using the Runge-Kutta Method and illustrated via computer simulations. The controllers devised in this research can solve specific and targeted motion control problems of smart cities' modern mechanical systems. The unanchored linear manipulator could be used in various disciplines where pick-and-place, assembly, material handling, and surgical procedures are required.

1. Introduction

The quest to achieve reduced production costs and boost productivity has provided an opportunity for technology to contribute positively towards the industrial sector and reshape manufacturing operations. In this digital age, industrial companies invest in research that offers solutions to meet the increasing demands of manufacturing and helps improve productivity in a short time. In the manufacturing industry, several production tasks that demand precision and repeatability have been taken over by robots [1]. Since the introduction of modern industrial robots in the 1950s, there have been significant improvements in technology, in particular, robotics technology [2]. Robots are highly valued in the manufacturing industry for several attributes such as reliability, predictability, precision, repeatability, and ability to operate in unsafe working environments [1,3,4].

---

* Corresponding author.
  E-mail address: sandeep.a.kumar@usp.ac.fj (S.A. Kumar).

Applications of robots in industrial operations have enabled many tasks to be performed in known, partially known, and unknown environments [4,5]. As labor costs rise and competition for low-wage overseas locations increases, more manufacturers employ robot technologies to perform specific tasks [6]. Some popular industrial robots that are utilized in pick and place and assembly line applications include delta robots, cartesian robots, SCARA robots (Selective Compliance Assembly Robot Arm), and cylindrical robots [7]. Cartesian robots, along with polar robots, are also relied upon to perform material handling tasks due to their ability to handle heavy loads [8,6]. Furthermore, to achieve high precision operations, cartesian robots and articulated robots are commonly used as a result of their high flexibility [6]. However, due to their ability to handle difficult and dangerous tasks, the robotic arm can be regarded as one of the most common manufacturing robots [9–11]. The many advantages of robotic arm guarantee its high usage to meet the demands of the industrial sector. These advantages include its contribution to improved production capacity, repeatability, and capability of working faster and more accurately than any human worker. In addition to minimizing the usage of floor space, an industrial robotic arm enhances the quality of product and work environment [12]. From tasks such as pick and place [10], machine tending [7], assembling [6] and material handling [8], robotic arms have been making industrial operations efficient and cost effective for manufacturing companies.

As described in [13], a robotic arm is an open or closed kinematic chain of rigid links interconnected by movable joints; the two commonly used being revolute and prismatic. Robotic arms are traditionally mounted to rigid structures as they perform specific tasks in constrained work environments. As a result, the arm's movement would not affect the position of its mount, and the functional space in which its task is performed would remain constant. Such manipulators are commonly known as anchored arms and typically consist of a power supply, controllers, and robot manipulator as demonstrated in [2] and [14]. On the other hand, an unanchored arm consists of a robotic arm mounted on a mobile base platform. Several modern applications have benefited from unanchored manipulators, including medical services from wheelchair robots [15], food delivery services from Segways [16], and the transportation sector from Uber services [17]. Moreover, the demands of tasks that include repeatability, reduced variability, quality expectations, and lower manufacturing costs have paved the way for unanchored robotic arms to be included in real-life applications such as mining, forestry, exploration, and military [18]. While specific robotic arms offer the best cost investment as they can be reprogrammed or repurposed to meet product variety and life cycles, linear robots, in particular, offer a more versatile solution for these challenges [19,7].

Linear robots are industrial robots that move only in a straight line instead of rotating in all directions [20]. Depending on the application, linear robots can handle tasks that require ultimate precision and repeatability with ease, boasting great versatility in moving up and down, left and right, or back and front accurately and efficiently. Linear robots with horizontal components supported at both ends can be categorized as Gantry robots [7]. Linear robotic systems have higher accuracy as there are no rotating axes and offer an ideal automation solution for accomplishing complex, repetitive tasks. Unlike other autonomous systems, linear mechanical systems are flexible to fulfill specific requirements and can be efficiently reprogrammed to meet the unique demands of the robotic workspace. Furthermore, linear robots usually are more economical than other automated systems, such as an articulated arm or SCARA [7].

Since the motion of linear robots is in the prismatic or linear directions, they can also be referred to as linear manipulators. The key advantages of these manipulators are that the robot's structure allows for quick movement with high repeatability, minor use of floor space, and a larger load capacity due to structural rigidity [12]. In addition, the long reach of the robotic arm in linear manipulators can lead to improved performances in industrial applications. However, as rightfully pointed out by [21], a significant impact on the overall performance, including safety and acceleration, of the manipulator as well as the success of the application depends on its payload. For instance, a pick and place robot must be able to lift the heaviest item in the workspace, fully extend its arm and place the said item precisely. Some everyday operations of linear manipulators in industries include material handling [8], pick and place [10], welding [22], painting [2], packaging [7], and assembly line solutions [6].

Apart from the vast contributions of robotic systems in industrial applications, one open question remains on how to improve the effectiveness of the manipulator by guiding it to perform tasks efficiently without difficulty and interruptions, given constrained workspaces. To resolve this, a geometric robotic problem, known as the robot path planning problem, has been continuously addressed by researchers over the years with various algorithms [23]. In other words, the desired solution for the robot findpath problem in a workspace cluttered with obstacles is a collision-free trajectory. Researchers utilize various techniques, strategies, and methods to solve this problem. These methods can be commonly categorized as Neural Networks [24], Graph Search Technique, Artificial Potential Field Method, heuristic based approaches [25] and Hybrid Systems [26]. However, due to the disadvantages attached to various algorithms and the continuously evolving needs of real-life applications, the search for better algorithms still prevails [27].

This paper is inspired by the gap noticed in the literature on efficient use of an *n*-link robotic arm mounted on a mobile linear slider to perform assigned tasks within its workspace. The individual controls of the robotic arm and the base link, in the form of a slider moving either horizontally or vertically along a rail, will be developed. While the mobile slider moves in a linear direction, the articulated arm moves in a two-dimensional plane, thus giving a two-dimensional motion of the entire system in effectively reaching the complete workspace. Such a system combines the advantages of mobile platforms and robotic arms and combines their significant strengths. For instance, the mobile linear slider extends the arm's reachability by advancing either horizontally or vertically along a rail towards an unreachable target, whereas the robotic arm offers several operational functionalities. Thus, the linear manipulator provides a dual advantage of mobility offered by the manipulator's mobile platform and agility of the end-effector. A set of stabilizing nonlinear, time-invariant, acceleration-based, continuous control laws will be developed using LbCS to navigate the linear manipulator system while obeying system constraints and singularities and simultaneously avoiding fixed solid barrier

obstacles in a two-dimensional bounded workspace. LbCS has been successfully implemented to guarantee operational need of the control systems presented in [28] and [29], and the asymptotic stability. The significant contributions of this paper are:

1. *design of a new modified linear manipulator mechanical system representing a unique combination of a linear robotic system integrated into a rail system.* This modification of the robotic arm concept and the two-step switch movement enables the linear slider to extend the arm's workspace by advancing linearly along the rail towards an elusive target with increased reachability. In comparison, the anchored robotic arm systems mentioned in [13,30,18] offer a restricted workspace and minimal operational functionalities of the end-effector in performing designated tasks. The proposed unanchored linear manipulator can have real-world applications in industrial sectors requiring process repeatability tasks like material handling and pick-and-place.

2. *design of the acceleration controllers from a Lyapunov function that facilitates a two-step switch movement of the mobile slider and the linear system's n-link robotic arm for increased reachability in the workspace.* From the authors' viewpoint, such stabilizing acceleration-based controllers for an *n*-link linear manipulator in the sense of Lyapunov are derived for the first time. The acceleration-based controllers guarantee smooth motion and trajectory when compared to velocity-based systems, which give rise to a sharp change in angular velocities resulting in unsteady motion [31,32]. The controllers developed in this research can be extended to solve motion control problems in various situations and concepts, such as the smart city where heterogeneous robotic systems need to be operationalized.

In Section 2, a discussion of the literature review is given. Next, section 3 briefly describes the Lyapunov-based Control Scheme, while Section 4 presents the system modeling of an *n*-link robotic arm mounted on a linear manipulator. Next, Section 5 provides the find-path problem for the linear manipulator. In Section 6, the stability of the mechanical system is analyzed. Then, Section 7 presents the simulation results. Finally, discussion and conclusive remarks are provided in Section 8 and Section 9, respectively.

2. Literature review

High performances of robotic manipulators when compared with the human arm motivated the development of new mechanical structures. This literature survey provides an overview of robotic arms, whereby an outline of developments from the first generation to the modern robotic arms comprising *n*-links is discussed. Moreover, practical applications of *n*-link robotic arms in planar robotic systems and linear manipulators are emphasized with their specific algorithms.

The foundation of industrial robotics lies in the development of robotic arms. Despite the recent advancements and development of robotic arms due to modern technology, a historical review discloses that robotic arms have been in existence for around 500 years. According to [33], Leonardo da Vinci designed the first sophisticated robotic arm in 1495 with four degrees of freedom and an analog onboard controller supplying power and programmability. This discovery eventually found its destination in the medical industry in 2000, resulting in the design of a robotic surgical system known as the 'da Vinci Surgical System'. Depending on the model, the da Vinci System consists of three to four interactive robotic arms controlled by a surgeon from a console to facilitate certain surgical operations [34]. However, the evolution of modern industrial robotic arms gained momentum in the 1950s, as researchers set up companies that could manufacture robots for industrial applications. In 1959, Unimate introduced its first robotic arm that was invented by George Devol and marketed by Joseph Engelberger [2,35]. However, due to difficulties experienced in reprogramming, these arms could only be used to accomplish single tasks like extracting parts from a die-casting machine [35]. In subsequent years and decades thereafter, an abundance of work was done within the framework of robotic arms [36,11]. Due to operational, technological and financial challenges, the tasks that the first generation robotic arms were capable of performing were necessarily relatively trivial, such as spot-welding, loading-unloading, or simple material handling operations [6].

Along with accomplishing tasks, modern mechanical applications require virtual models to be developed and simulated before implementation. As a result, the literature indicates a substantial upgrade of unanchored robotic arms from single to *n*-link systems. Fayazi et al. [37] presented a single-link flexible arm that has the potential to aid the analysis of impact-induced structural vibrations for structural analysis and dynamic modeling. A fabricated planar 2-link vertical robotic arm apparatus was used by Wilson et al. [38] in 2016 for the successful experimental testing of the controllers and trajectory tracking for the benefit of the manufacturing industry. Chaitanya et al. [39] in 2017 used a heuristic search algorithm to optimize a 2-link revolute robotic manipulator for maximization of workspace covered by its end-effector. Nakalo et al. [40] in 2018 demonstrated that a 3-link robotic arm mounted on base link comprising an underwater vehicle-manipulator system can be effectively utilized in ocean exploration. Furthermore, the kinematics-based analysis of a 4-link robotic arm was studied by Lee et al. [41] in 2019 whereby a rigorous torque analysis of the mechanism was carried out. It was observed that the proposed robotic arm correctly followed the desired motions by the controller.

To improve the performance of revolute robotic arm manipulators, researchers increased the number of links in the system, resulting in the publication of several articles. Iqbal et al. [42] in 2012 kinematically analyzed and modeled the workspace of the commonly used 6-DOF, 5-link revolute arm manipulator called ED7220C. Unfortunately, in their research, position precision could not be acquired ideally due to inappropriate joint angles arising from non-linearity in mapping angles and improper mechanical coupling of the joints [18]. Asadi et al. [43] in 2019 utilized a 6-link revolute arm on a mobile unmanned ground vehicle (UGV) with a stereo camera that was capable of removing obstacles across the UGV's path. In the investigation, although the 6-DOF manipulator could follow the orientation and location of the detected objects, the robotic arm encountered difficulties reaching the object by tracking the predetermined orders.

Multilink planar robots are interesting systems in the fields of control and robotics; however, in recent years, very little research attention has been given to multilink underactuated planar robotic arms [7,44,8]. For different actuator-sensor configurations, the

linear controllability and observability of an n-link revolute planar robotic arm with all links moving in the same vertical plane were investigated by Liu et al. in 2016 [8]. The findings revealed that in the control of load-bearing robots and navigation through cluttered search and rescue environments, stability, along with controllability and effective performance, are vital components. In 2018, Xin [45] refined and expanded the work done in [8] and solved an open problem of that time, based on the linear strong structural controllability and observability of a robotic arm with active intermediate joints. Xin proved that when neither the first nor last joint of the n-link underactuated revolute planar robotic arm is active, such an arm is linearly strongly structurally controllable and observable if and only if there are at least two active adjacent joints.

Moreover, De Luca et al. [44] attempted to solve the trajectory planning and control problem of n-link planar robotic arms with passive rotational last joint in the unifying framework of dynamic feedback linearization, both in the absence and presence of gravity. Experimenting on the position of the center of percussion of the last link as the linearizing output, the results showed that swing-up maneuvers and smooth trajectories for any initial and desired final state of the robotic arm under gravity could be easily obtained. Shafei et al. [46] utilized a multivariable kinematic controller to obtain the trajectory tracking control and dynamic modeling of a robotic manipulator consisting of n-rigid links connected by revolute joints installed on an autonomous mobile platform. A predictive control process was taken to determine appropriate input control torques and optimum velocities for the robotic system in the existence of model uncertainties. However, as pointed out in [47] and [18], executing safe motion of manipulators of various sizes and geometry is challenging yet crucial for any robotic system.

Sharma et al. in 2012 presented a set of continuous acceleration control laws, derived from the Lyapunov-based Control Scheme, to tackle the multi-task problem of navigation and steering of a single [48], and later, for multiple n-link doubly nonholonomic mobile manipulators [3]. The same technique was used in 2018 by Sharma et al. [5] whereby continuous time-invariant nonlinear control laws were used together with a variant of the leader-follower scheme to establish and mobilize a globally rigid formation of a team of n-link doubly nonholonomic mobile manipulators within an obstacle cluttered environment. The pivotal idea behind these studies is the design of an appropriate Lyapunov function, which acts as an artificial potential field function, to address stability issues of the robotic system. The integrated Lyapunov Method has been effectively utilized in finding feasible solutions to MPC problems of robotic systems in different environments with various applications as seen in studies such as [49], [5], [48] and [3]. Along with MPC, various other attributes such as asymptotic regulation, load capacity, positioning, weight, and size of the links must be considered to achieve a sustainable design of flexible and versatile robotic manipulators [12].

The flexibility and versatility of linear manipulators have made significant contributions to material handling and pick and place applications. These attributes can be seen in the INDEVA Linear Manipulator [50] as it ergonomically supports operators in picking up and positioning offset heavy reels. The linear manipulator can also be mounted on an electric transpallet, allowing the operators to easily move the manipulator to any work area where reel handling is required. In regards to pick and place operations, Motoman robots ranging from 2 kg payload capacity to 10 kg with cycle-times as high as 150 pick cycles per minute are common [10]. In terms of speed, Delta Robots, if placed in a row over a conveyor belt, equipped with MotoSight 2D Camera and MotoPick Software, can achieve pick rates in the range of 150 to 200 parts/minute per picking line. SCARA-Robots, which are horizontally articulated robots, are capable of performing extraordinary high pick rates as well and are good choice for up/downwards pick and place jobs on a flat table [7]. The small 6-axis MotoMin robots are employed in situations where the pick direction is different from the place direction [10].

Although the literature for the design and implementation of robotic arm systems is vast and rapidly expanding, only a small number of publications on linear manipulators could be obtained from a comprehensive literature search. Just recently, Yu et al. [51] presented an ultrasound probe that was fixed on an unanchored robotic arm to scan COVID-19 patients during the outbreak in 2020 with the possibility of popularizing it for diagnosis and monitoring of COVID-19 cases in clinical practice. While the demand for linear manipulators in real-life applications is expanding consistently, this paper addresses the MPC of linear manipulators with the aim of filling the existing gap in the literature. Using the method of LbCS, a new modified unanchored manipulator proposed in this paper, consisting of n-links, can perform assigned tasks while navigating to its target. In addition, the linear robotic arm manipulator is capable of repositioning its base link to a desired location in the workplace due to changes in work requirements. This two-step switched motion technique of the new modified linear robotic system can positively impact real-life industrial applications requiring pick and place, assembly, material handling, packaging, and even surgical operations.

3. Lyapunov-based control scheme

The Lyapunov-based Control Scheme (LbCS) forms a basis of MPC of autonomous robots and can be classified under the artificial potential field technique often utilized in robotics research [48]. Operations within the control scheme are guided by the principle of the Direct Method of Lyapunov. The fundamental concept of the control scheme is to create an suitable Lyapunov function that serves as an energy function in the form of total potentials [52]. In this method, the Lyapunov function or total potentials is employed to design relevant velocity-based controls or acceleration-based controls to guide the robots to their corresponding targets.

The system's total potentials consists of two types of fields, namely repulsive field and attractive field. The ruling principle behind the potential method is to assign a repulsive field to each obstacle and an attractive field to the target [15,53]. The Lyapunov function is the sum of each and every repulsive and attractive potential functions [54,48], thus establishing a basis for deriving the controllers of a linear manipulator. The repulsive potential function is a ratio of a positive tuning parameter to the obstacle avoidance function. After the whole workspace is disseminated with negative and positive fields, the concept of steepest descent influences the direction of motion of the manipulator [3]. Moreover, for the linear manipulator, the gradient of the total potentials determines the velocity
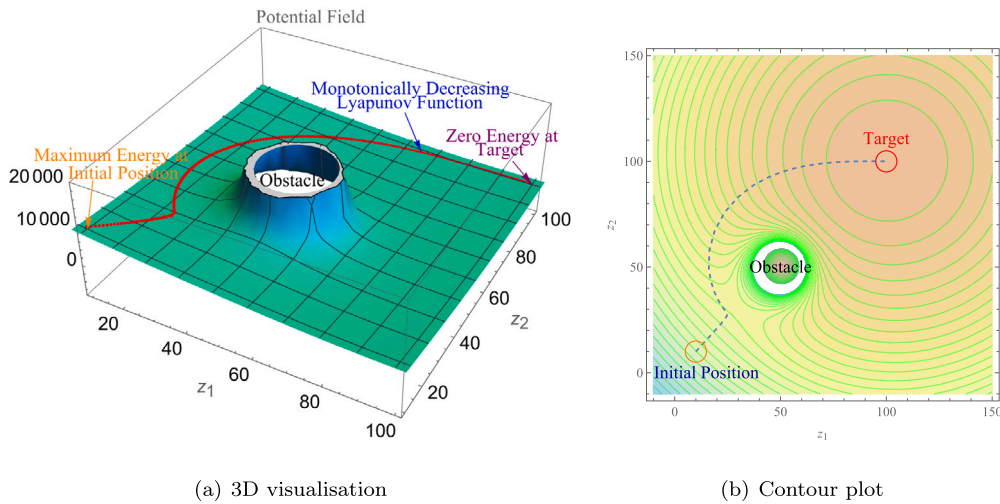
(a) 3D visualisation

(b) Contour plot

Fig. 1. A demonstration of the Lyapunov-based Control Scheme.

with which the manipulator will move. The control laws are created such that the total potential is decreasing for all $t \geq 0$ and disappears to zero as $t \to \infty$ [49].

The advantage of the LbCS framework is that it gives simple and effective means of scheming continuous time-variant controllers for autonomous robots and easier treatment of obstacles and constraints [55]. The LbCS has been used for a spectrum of issues such as obstacle avoidance, point and posture stabilization, swarming and path tracking to solve motion problems associated with different mechanical systems [49,23,53,31,5].

Fig. 1 shows the 3D visualization and contour plot of a Lyapunov function devised over the workspace for a manipulator whose original position is at (10,10). The dotted line depicts the manipulator's trajectory from its original position to its target location (100,100), which demonstrates the manipulator avoiding an obstacle located at (50,50) with a radius of 10.

4. System modeling

In this paper, an n-link revolute robotic arm mounted on a linear slider in a 2-dimensional plane, as shown in Fig. 2, is considered. The planar articulated arm is unanchored, consisting of n revolute links with the last link connected to an end-effector. The arm of the system operates in the $z_1 z_2$-plane as it performs assigned tasks in a two-dimensional bounded workspace. The linear slider undergoes horizontal or vertical motion along a rail, which is of length $(r_l - \kappa)$, on the z_1-axis and performs linear motion to ensure the end-effector is able to reach the target and perform assigned tasks within the workspace. As a result, the robotic arm manipulator horizontally or vertically repositions its base link to a desired location due to change in work requirements. The non-holonomic constraints of the mobile base, which is the slider mounted on the rail, are redundant because the autonomous slider has no lateral movement. Considering the n-link robotic arm, the ith revolute link on the n-link robotic arm has a length of l_i and an angle position of $\theta_i(t)$ with respect to the z_1 axis. At time t, the final link has a length of l_n and an angular position of $\theta_n(t)$. The position $(x(t), y(t))$ of the end-effector of the linear manipulator at time t is given by the equations:

$$x(t) = x_1(t) + \sum_{i=1}^{n} l_i \cos\left(\sum_{m=1}^{i} \theta_m(t)\right),$$

$$y(t) = \sum_{i=1}^{n} l_i \sin\left(\sum_{m=1}^{i} \theta_m(t)\right).$$

The motion of the n-link revolute robotic arm with an end-effector can be described by constructing a system of differential equations. At $t \geq 0$, $\mathbf{x} = (x(t), y(t))$ denotes the position of the end-effector of the n-link robotic arm with $\theta_n = \theta_n(t)$ as the orientation angle. Let $\theta_i = \theta_i(t)$ be the angular orientation of the ith link for $i \in \{1, 2, 3 \ldots, n\}$. Also, the variables in this paper are designated as:

$$x(t) = \text{the } x-\text{coordinate of the end}-\text{effector position}$$

$$y(t) = \text{the } y-\text{coordinate of the end}-\text{effector position}$$

$$x_1(t) = x-\text{coordinate of the base of link 1 mounted on the slider}$$

$$\theta_i(t) = i^{th} \text{ link's angular position for } i \in \{1, 2, \ldots, n\}$$

$$\omega_i(t) = i^{th} \text{ link's angular velocity for } i \in \{1, 2, \ldots, n\}$$

$$\sigma_i(t) = i^{th} \text{ link's angular acceleration for } i \in \{1, 2, \ldots, n\}$$
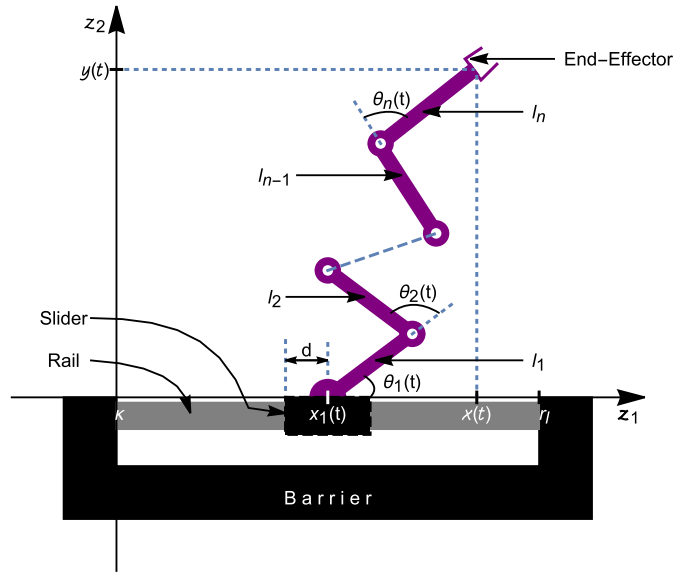
Fig. 2. A two-dimensional schematic representation of a revolute robotic arm affixed to a linear slider.

$v(t) =$ is the instantaneous velocity of the base link slider

$\alpha(t) =$ is the instantaneous acceleration controller of the slider

$\forall t \geq 0$.

Consider an n-link revolute robotic arm mounted on a linear slider in a 2-dimensional plane, with the linear slider undergoing horizontal motion on the z_1-axis along a rail fixed on a barrier. The kinematic model of the system, suppressing t, is:

$$
\left.
\begin{aligned}
\dot{x} &= v - \sum_{i=1}^{n} \omega_i \left(y - \sum_{j=1}^{i-1} l_j \sin \left(\sum_{m=1}^{j} \theta_m \right) \right), \\
\dot{y} &= \sum_{i=1}^{n} \omega_i \left(x - \sum_{j=1}^{i-1} l_j \cos \left(\sum_{m=1}^{j} \theta_m \right) \right), \\
\dot{\theta}_i &= \omega_i, \\
\dot{x}_1 &= v, \\
\dot{\omega}_i &= \sigma_i, \\
\dot{v} &= \alpha.
\end{aligned}
\right\}
\tag{1}
$$

Let $\mathbf{x}_0 = (x_0, y_0)$. The state vector of the system, suppressing t, is $\mathbf{x} := (x, y, x_1, \theta_1, \theta_2, \ldots, \theta_n) \in \mathbb{R}^{n+3}$. Also, let $\mathbf{x}_0 := \mathbf{x}(t_0) := (x_0, y_0, x_{10}, \theta_{10}, \theta_{20}, \ldots, \theta_{n0}) \in \mathbb{R}^{n+3}$. This study is a theoretical exposition into the implementation of LbCS in solving the MPC problem of linear manipulators, focusing on the kinematic analysis of the new modified linear manipulator shown in Fig. 2, and the dynamic modeling of this system is open for research.

5. Findpath problem

Consider a 2-dimensional workspace of an n-link robotic arm manipulator mounted on a linear slider moving horizontally along a rail. The linear manipulator governed by system (1) has to navigate to its target while undergoing linear horizontal motion. The end-effector of the n-link revolute manipulator has to maneuver to a reachable destination without any motion by the slider. However, to navigate to an unreachable target within the workspace, the slider has to move horizontally along the rail when required and facilitate the end-effector in accomplishing the assigned task by reaching its target. This technique ensures that the robotic arm manipulator is capable of repositioning its base link to a desired location in the workplace due to change in work requirements. While operating on a linear axis, the mobile platform offers an extended configuration space for the robotic arm with options to carry out assigned tasks.

Definition 5.1. *The target for the n-link robotic arm end-effector is disk-shaped, having a center $\mathbf{x}_T = (a, b)$ and radius r_T. It is described as:*

$$T = \{(z_1, z_2) \in \mathbb{R}^2 : (z_1 - a)^2 + (z_2 - b)^2 \leq r_T^2 \}.$$

Definition 5.2. *The position of the base of link 1 mounted on the slider is described as* $\boldsymbol{x}_1 = (x_1, 0)$, *with an initial position* $\boldsymbol{x}_{10} = (x_{10}, 0)$. *The target of the slider is defined as:*

$$\boldsymbol{x}_{T1} = (\eta, 0).$$

5.1. Slider target attraction function

For attraction to the slider target $\boldsymbol{x}_{T1}$, an attractive function will be utilized which is not only a measure of the distance between the base of link 1 mounted on the slider and the barrier but is also a measure of its convergence to the target. The target attraction function for the slider is proposed to be:

$$A(\boldsymbol{x}) = \frac{1}{2} \left(\|\boldsymbol{x}_1 - \boldsymbol{x}_{T1}\|^2 + v^2 + \sum_{i=1}^{n} \omega_i^2 \right).$$

5.2. End-effector target attraction function

Employing the radically unbounded function:

$$B(\boldsymbol{x}) = \frac{\xi}{2} \left(\|\boldsymbol{x} - \boldsymbol{x}_T\|^2 \right)$$

will guarantee that the robotic arm's end-effector will converge to its equilibrium position.

5.3. Stationary obstacle avoidance

For the slider to avoid both sides of the stationary solid barrier on which the rail is fixed, the following obstacle avoidance function will be used for the linear manipulator:

$$W_1 = x_1 - d - \kappa, \text{and } W_2 = r_l - x_1 - d,$$

where d is half the length of the slider, κ is the x-coordinate at the beginning of the rail, and r_l is the x-coordinate at the end of the rail. Both the functions mentioned above are positive in the workspace, that is, $W_1, W_2 > 0$. For some constants $\gamma_i > 0, i \in \{1, 2\}$ where γ_i is the obstacle avoidance parameter, consider the effect of the ratios

$$\frac{\gamma_1}{W_1}, \frac{\gamma_2}{W_2}.$$

At large distances between the base of link 1 mounted on the slider and the fixed solid barrier, the ratios are negligible. When the slider linearly approaches the barrier obstacle, the obstacle avoidance function W_i decreases, which causes an increase in the ratio, and thus, γ_i represents a measurement of the strength of interaction between the slider and the barrier. Thus, the ratio acts as a repulsive-potential, which increases in the value corresponding to avoidance as the slider approaches the fixed barrier.

5.4. Artificial obstacle avoidance functions

5.4.1. Angular limitations and restrictions of revolute links
All singularities generated by the manipulator's revolute arms geometric composition needs to be considered. The first link of the robotic arm cannot rotate entirely to the uniform surface of the slider on which it is mounted while rotating both clockwise and anti-clockwise. The singularities of the first link occur when $\theta_1 \in \{\phi, \pi - \phi\}$. To avoid the singularities of the first link, the below functions are proposed:

$$W_3 = \phi - |\theta_1| \text{ and } W_4 = \pi - \phi - |\theta_1|.$$

Similarly, the second link cannot completely fold on the first link while rotating both anti-clockwise and clockwise. The singularity of the second link occurs when $\theta_2 = |\theta_{2_{max}}|$, which also occurs for the other revolute links of the robotic arm. Hence, it can be generalized as $\theta_i = |\theta_{i_{max}}|$ for $i \in \{2, 3, \dots, n\}$.

The following functions are considered to avoid interior singularities of the remaining links:

$$W_{3+i} = \theta_{i_{max}} - |\theta_i|, \text{ for } i = \{2, 3, .., n\}.$$

5.4.2. Restriction on the linear velocity of slider
The base of link 1 mounted on the slider must move smoothly along the rail. Therefore, to guarantee that the linear slider adheres to the velocity restrictions while in motion, the following function is introduced:

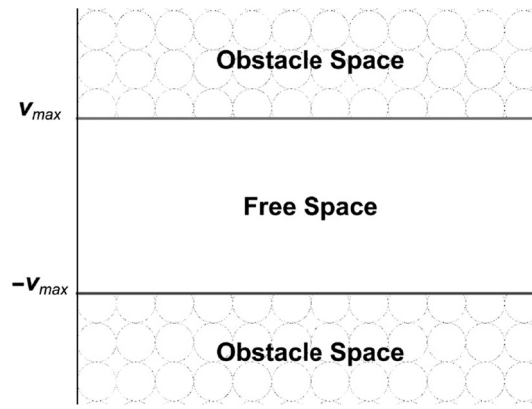$$F = \frac{1}{2} \left(v_{max}^2 - v^2 \right), \tag{2}$$

Fig. 3. The obstacle space forms the artificial obstacles that restrict the linear velocity of the slider.

where v_{max} is the maximum linear velocity that the slider can achieve. The velocity of the slider is bound by the restrictions imposed by equation (2). The repulsive potentials of the maximum linear velocity of the slider can therefore be treated as artificial obstacles as illustrated in Fig. 3.

5.4.3. Restrictions on the angular velocities of revolute links

The angular velocities of the revolute links must be controlled to facilitate a precise trajectory in navigating the target. Therefore, the following function is utilized to control the angular velocities of the robotic arm:

$$G_i = \frac{1}{2} \left(\omega_{i_{max}}^2 - \omega_i^2 \right),$$

where $\omega_{i_{max}}$ is the maximum angular velocity of the ith revolute link for $i = \{1, 2, 3, \ldots, n\}$.

5.5. Auxiliary function

The following auxiliary function is considered to ensure that the linear manipulator system converges to its target and guarantees that the nonlinear acceleration controllers vanish at the target:

$$H(\boldsymbol{x}) = \frac{1}{2} \left(\|\boldsymbol{x}_1 - \boldsymbol{x}_{T1}\|^2 \right) + \frac{\xi}{2} \left(\|\boldsymbol{x} - \boldsymbol{x}_T\|^2 \right).$$

The auxiliary function, $H(\boldsymbol{x})$, will be multiplied to the total repulsive potential in accordance with the LbCS.

5.6. Multiple Lyapunov functions

To guarantee the convergence of the n-link linear manipulator to its prescribed target, appropriate control parameters need to be introduced. Let λ, β_i and γ_i be elements of $\mathbb{R}^+$, which are the control parameters. Define for $i \in \{1, 2, 3, \ldots, n\}$ a Lyapunov function of the form,

$$L(\mathbf{x}) = A(\boldsymbol{x}) + B(\boldsymbol{x}) + H(\boldsymbol{x}) \left(\frac{\lambda}{F} + \sum_{i=1}^{n} \frac{\beta_i}{G_i} + \sum_{i=1}^{n+3} \frac{\gamma_i}{W_i} \right), \tag{3}$$

where the target attraction parameter is of the form,

$$\xi = \begin{cases} \varepsilon \left((x_1(t) - \eta)^2 - c^2 \right)^2, & (x_1(t) - \eta)^2 \le c^2 \\ 0, & otherwise. \end{cases}$$

The end-effector can reach the target if and only if:

$$\eta \le c \le \left(\sum_{i=1}^{n} l_i \right)^2 - b^2.$$

The function ξ will be evaluated initially at $t = 0$, and then it will be updated as the slider propels towards the target. The purpose of this function is to allow the slider to move along the rail from its initial position towards an unreachable target from where the end-effector can reach out and carry out its designated task. Thus, the linear manipulator's motion is continuous for all time $t \ge 0$, and the end-effector does not get attracted to its target until the slider's final position is less than a distance of c from the end-effector target. The particular form of ξ indicates that the linear manipulator is navigating in its workspace, hence ensuring that the stabilizing acceleration-based controllers to be proposed are continuous.

5.7. Controller design

Within the framework of LbCS, all the repulsive and attractive potential functions are combined to form a total potential for system (1). The control design will either decrease or increase the number of outputs or inputs based on the number of links and remains the same for manipulators with different link numbers. The design of the controllers is generic enough to accommodate any number of links as per the requirements of the intended application. Along a trajectory of system (1),

$$\dot{L}(x) = \dot{A}(x) + \dot{B}(x) + \dot{H}(x)\left(\frac{\lambda}{F} + \sum_{i=1}^{n}\frac{\beta_i}{G_i} + \sum_{i=1}^{n+3}\frac{\gamma_i}{W_i}\right) - H(x)\left(\frac{\lambda\dot{F}}{F^2} + \sum_{i=1}^{n}\frac{\beta_i\dot{G}_i}{G_i^2} + \sum_{i=1}^{n+3}\frac{\gamma_i\dot{W}_i}{W_i^2}\right),$$

which can be rearranged, upon collecting terms with v, and ω_i, as

$$\dot{L}(x) = fv + \sum_{i=1}^{n}f_i\omega_i,$$

where the functions f and f_i, on suppressing $\mathbf{x}$, are defined as:

$$f = \alpha + \frac{\partial L}{\partial x_1} + \frac{\lambda H}{F^2}\alpha,$$

$$f_i = \sigma_i + \frac{\partial L}{\partial \theta_i} + \frac{\beta_i H \sigma_i}{G_i^2}.$$

With the necessary substitutions carried out, and introducing the convergence parameters $\delta_1 > 0$ and $\delta_{i+1} > 0$ for $i \in \{1,2,3,...,n\}$ such that

$$\dot{L} = -\delta_1 v^2 - \sum_{i=1}^{n}\delta_{i+1}\omega_i^2 \leq 0,$$

then the controllers of the linear manipulator system are obtained as:

$$\left.\begin{array}{l}\alpha = -\frac{F^2}{\lambda H}\left(\delta_1 v + \frac{\partial L}{\partial x_1}\right), \\[2mm] \sigma_i = -\dfrac{1}{1+\sum_{i=1}^{n}\frac{\beta_i H}{G_i^2}}\left(\sum_{i=1}^{n}\delta_{i+1}\omega_i + \sum_{i=1}^{n}\frac{\partial L}{\partial \theta_i}\right),\end{array}\right\} \tag{4}$$

where α is the acceleration controller of the linear slider, and σ_i is the controller of the angular acceleration of the ith link revolute arm.

6. Stability analysis

Lyapunov functions are normally utilized to prove that an equilibrium point of a robotic system is Lyapunov stable. The control laws have been extracted from the Lyapunov function given in equation (3), $L(\mathbf{x})$, which appropriately combined the system singularities, dynamic constraints, attractive and avoidance functions. It is assumed that

$$\mathbf{x}_e := (x_e, y_e, x_{1e}, \theta_{1e}, \theta_{2e}, \dots, \theta_{ne}) \in \mathbb{R}^{n+3} \in D\big(L(\mathbf{x})\big)$$

is at least an equilibrium point of system (1). By letting $\dot{L}(\mathbf{x}) = f(\mathbf{x})$, it can be shown that $f(\mathbf{x}_e) \equiv 0$, making $\mathbf{x}_e$ a feasible equilibrium point. With respect to system (1),

$$\dot{L}(\mathbf{x}) = -\delta_1 v^2 - \sum_{i=1}^{n}\delta_{i+1}\omega_i^2 \leq 0,$$

$\forall\, \mathbf{x} \in D\big(L(\mathbf{x})\big).$

Stability means that any solution of system (1) starting close to the equilibrium point $\mathbf{x}_e$ remains near it at all times. Therefore, it is evident that $\mathbf{x}_e$ is an equilibrium point of system (1), and $L(\mathbf{x})$ is a Lyapunov function on $D\big(L(\mathbf{x})\big)$ that guarantees its stability. This analysis is appropriately summed up in Theorem (6.1) below:

Theorem 6.1. *The equilibrium point $\mathbf{x}_e$ of system (1) is stable provided α and σ_i for $i = \{1,2,3,\dots,n\}$ are defined as in (4).*

Proof.   1. $L(\mathbf{x})$ is defined, continuous and positive on the domain given as

$$D\big(L(\mathbf{x})\big) = \left\{\mathbf{x} \in \mathbb{R}^{n+3} : F > 0,\ G_i \geq 0\ \forall\, i = \{1,2,3,\dots,n\},\ W_k > 0\ \forall\, k = \{1,2,3,\dots,n+3\}\right\}.$$

2. $L(\mathbf{x}_e) = 0$, $\mathbf{x}_e \in D\big(L(\mathbf{x})\big)$.
3. $\dot{L}(\mathbf{x}) \leq 0$, $\forall\, \mathbf{x} \in D\big(L(\mathbf{x})\big)$. $\square$

Table 1
Table of parameters.

x-coordinate at the end of the rail	r_l
Origin of the 2-dimensional workspace and location of the initial fixed end of the rail	κ
Length of Slider	$2d$
Coordinate of Slider Target	$(\eta, 0)$
Number of revolute links	$n \in \mathbb{N}$
Lengths of revolute links	$l_i, i \in \{1, 2, \ldots, n\}$
Initial orientations of revolute links	$\theta_{i_0}, i \in \{1, 2, \ldots, n\}$
Initial position of slider	$(x_{1_0}, 0)$
Initial linear velocity of slider	v_0
Maximum linear velocity of slider	v_{max}
Initial angular velocity of revolute links	$\omega_{i_0}, i \in \{1, 2, \ldots, n\}$
Maximum angular velocity of revolute links	$\omega_{i_{max}}, i \in \{1, 2, \ldots, n\}$
End-Effector Target	(a, b)
Obstacle avoidance parameter	$\gamma_i, i \in \{1, 2, \ldots, n\}$
Linear velocity restriction parameter of slider	λ
Angular velocity restriction parameters of the revolute links	$\beta_i, i \in \{1, 2, \ldots, n\}$
Slider convergence parameter	δ_1
Revolute link angular velocity convergence parameters	$\delta_{i+1}, i \in \{1, 2, \ldots, n\}$

7. Results and simulations

The computer simulations were performed using Wolfram Mathematica 11.2 software to validate the results. A series of Mathematica commands were executed to obtain the simulation results. The system singularities, restriction avoidance, and convergence parameters must be defined before the proposed algorithm of the linear manipulator system is implemented.

The brute-force method is applied to set the control parameters. There can only be a unique set of initial conditions based on the target position to ensure a smooth trajectory of the linear slider and the robotic arm end-effector as the linear manipulator system tracks through the 2-dimensional workspace and eventually converges on the ultimate target. The mechanical system's dynamic constraints and singularities and the acceleration controllers allow the linear manipulator to trace the specified path. Although certain paths may not be feasible, the initial requirements and singularities will alter and depend on the path that will lead to the destination using the LbCS's steepest descent principle. Table 1 illustrates the parameters that have to be defined. The initial state of the linear manipulator system has to be defined in the sequence of commands to be executed. Using the RK4 method, system (1) was numerically simulated. The system's initial configurations $(x_0(0), y_0(0))$, η, d, κ, r_l, $x_{1_0}(0)$, and orientations $\theta_i(0)$ were generated at $t = 0$.

7.1. Scenario 1

This scenario considers a linear manipulator system comprising a 3-link revolute robotic arm mounted on a slider positioned initially at (4, 0). After the linear slider has reached its target located on its right by moving horizontally along the rail, the robotic arm end-effector should navigate through the workspace and reach its ultimate target. The numerical values of the convergence parameters, initial states, and control parameters used in the simulation are provided in Table 2. The initial configuration of the 3-link linear manipulator on the rail and the targets of the slider and end-effector are shown in Fig. 4(a). The motion of the linear slider along the rail, orientations of each of the three revolute links, and the trajectory of the end-effector of the robotic arm as it maneuvers the target are shown in Fig. 4(b). Fig. 4(c) illustrates the evolution of the Lyapunov function, L, which is monotonically decreasing as time evolves. The function's behavior indicates that the end-effector of the revolute arm is converging to its target. As the slider approaches its target, the linear velocity of the slider gradually decreases to zero as is shown in Fig. 4(d). The orientation angles and the angular velocities of the revolute links abiding the limitations and restrictions tagged to the robotic arm are illustrated in Fig. 5(a) and Fig. 5(b) respectively.

7.2. Scenario 2

This scenario considers a linear manipulator system comprising a 4-link revolute robotic arm, with different link sizes, mounted on a slider positioned initially at (25, 0). The linear manipulator has to maneuver to its ultimate target located on its left along a longer rail compared to Scenario 1. If the simulation uses different initial conditions, parameters or conditions than the prior scenario, those are listed in Table 3. The initial position of the 4-link linear manipulator on the rail, motion of the linear slider along the rail, orientations of each of the four revolute links, and the trajectory of the end-effector of the robotic arm as it maneuvers towards the target are shown in Fig. 6. The linear velocity of the slider, which is negative as the system is moving from right to left along the

Table 2

Numerical values of convergence parameters, initial states, and control parameters.

x-coordinate at the end of the rail	$r_l = 14$
Origin of the 2-dimensional workspace and location of the initial fixed end of the rail	$\kappa = 1$
Length of Slider	$2d = 2$
Coordinate of Slider Target	$(\eta, 0) = (12, 0)$
Number of revolute links	$n = 3$
Lengths of revolute links	$l_1 = l_2 = l_3 = 4$
Initial orientations of revolute links	$\theta_{1_0} = \frac{\pi}{2},\ \theta_{2_0} = -\frac{7\pi}{9}$ and $\theta_{3_0} = \frac{7\pi}{9}$
Initial position of slider	$(x_{1_0}, 0) = (4, 0)$
Initial linear velocity of slider	$v_0 = 0$
Maximum linear velocity of slider	$v_{max} = 1$
Initial angular velocity of revolute links	$\omega_{1_0} = \omega_{2_0} = \omega_{3_0} = 0$
Maximum angular velocity of revolute links	$\omega_{1_{max}} = \omega_{2_{max}} = \omega_{3_{max}} = 1$
End-Effector Target	$(a, b) = (14, 8)$
Obstacle avoidance parameter	$\gamma_1 = \gamma_2 = 0.002,\ \gamma_3 = \gamma_4 = \gamma_5 = \gamma_6 = 0.003$
Linear velocity restriction parameter of slider	$\lambda = 0.001$
Angular velocity restriction parameters of the revolute links	$\beta_1 = \beta_2 = \beta_3 = 0.005$
Slider convergence parameter	$\delta_1 = 10$
Revolute link angular velocity convergence parameters	$\delta_2 = \delta_3 = \delta_4 = 0.2$

(a) Initial positions and orientations   (b) Final positions and orientations

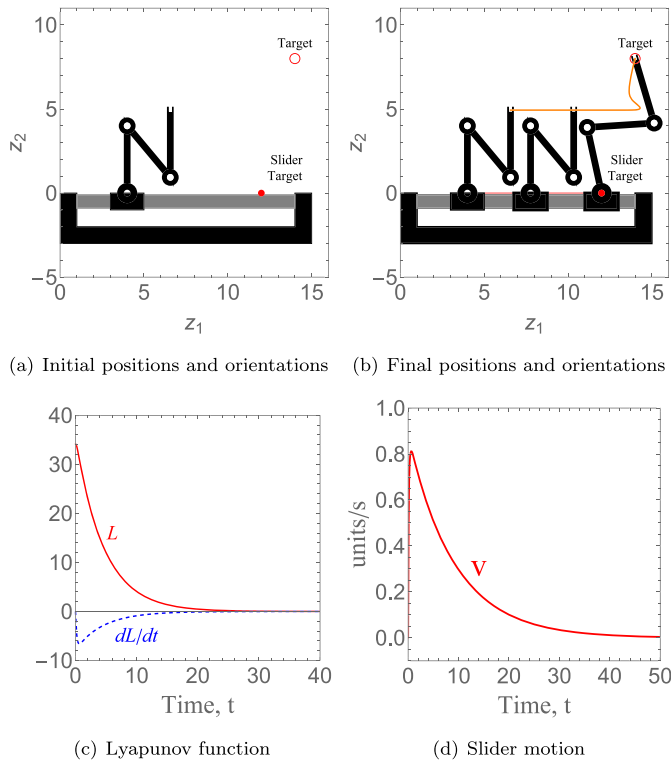(c) Lyapunov function   (d) Slider motion

Fig. 4. (a) Initial positions of the 3-link revolute robotic arm on the linear slider. (b) Positions of the 3-link revolute robotic arm on the linear slider at times $t = 0, 6$, and 3999, respectively. The end-effector's trajectory is traced in orange. (c) Monotonically decreasing Lyapunov function and its time derivative. (d) Linear velocity of slider.

z_1 axis, is shown in Fig. 7(a). The orientation angles and the angular velocities of the revolute links adhering the resstrictions and limitations tagged to the robotic arm are illustrated in Fig. 7(b) and Fig. 7(c) respectively. The behavior of the Lyapunov function, L, is similar to that of Scenario 1.

(a) Revolute link orientations   (b) Revolute link angular velocities
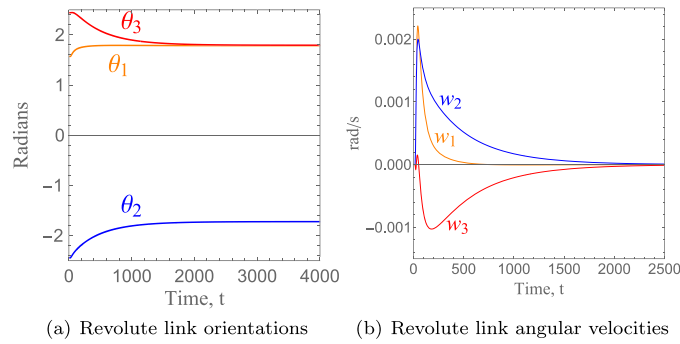
Fig. 5. (a) The revolute links orientations adhering to angular restrictions and limitations. (b) Angular velocities of the revolute links of the robotic arm.

Table 3
Numerical values of convergence parameters, initial states, and control parameters.

|	
x-coordinate at the end of the rail	$r_l = 28$
Length of Slider	$2d = 4$
Coordinate of Slider Target	$(\eta, 0) = (7, 0)$
Number of revolute links	$n = 4$
Lengths of revolute links	$l_1 = 5,\ l_2 = 4,\ l_3 = 3,\ l_4 = 2$
Initial orientations of revolute links	$\theta_{1_0} = \frac{\pi}{2},\ \theta_{2_0} = \frac{7\pi}{9},\ \theta_{3_0} = -\frac{7\pi}{9}$ and $\theta_{4_0} = \frac{7\pi}{9}$
Initial position of slider	$(x_{1_0}, 0) = (25, 0)$
End-Effector Target	$(a, b) = (1, 11)$
Obstacle avoidance parameter	$\gamma_1 = \gamma_2 = 0.002,\ \gamma_3 = \gamma_4 = \gamma_5 = \gamma_6 = \gamma_7 = 0.003$
Angular velocity restriction parameters of the revolute links	$\beta_1 = \beta_2 = \beta_3 = \beta_4 = 0.005$
Slider convergence parameter	$\delta_1 = 21$
Revolute link angular velocity convergence parameters	$\delta_2 = \delta_3 = \delta_4 = \delta_5 = 0.2$
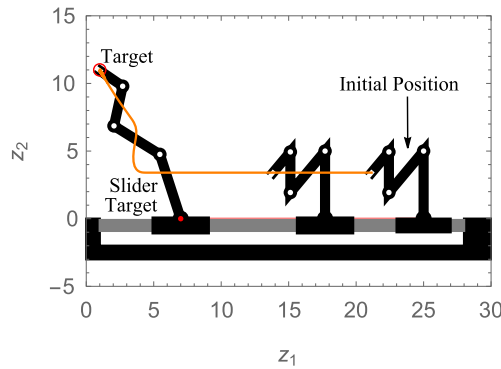
Fig. 6. Positions of the 4-link revolute robotic arm on the linear slider at times $t = 0, 10$, and 3999, respectively. The end-effector's trajectory is traced in orange.

7.3. Scenario 3

This scenario considers a linear manipulator system comprising a 5-link revolute robotic arm mounted on a slider positioned initially at $(4, 0)$. The linear manipulator has to maneuver to its ultimate target that is located beyond the size of the rail. The slider has to navigate to its target, thereafter, the revolute arm extends and opens up its links in order to reach the target. If the simulation uses different initial conditions, parameters or conditions than the prior scenarios, those are listed in Table 4. The initial position of the 5-link linear manipulator on the rail, motion of the linear slider along the rail, orientations of each of the five revolute links, and the trajectory of the end-effector of the robotic arm as it maneuvers to the target are shown in Fig. 8(a). The angular velocities of the revolute links abiding angular limitations and velocity restrictions are illustrated in Fig. 8(b). The behavior of the Lyapunov function, L, linear velocity of the slider, and the angular orientations of the revolute links are similar to those of Scenario 1.

(a) Slider Velocity

(b) Revolute link orientations

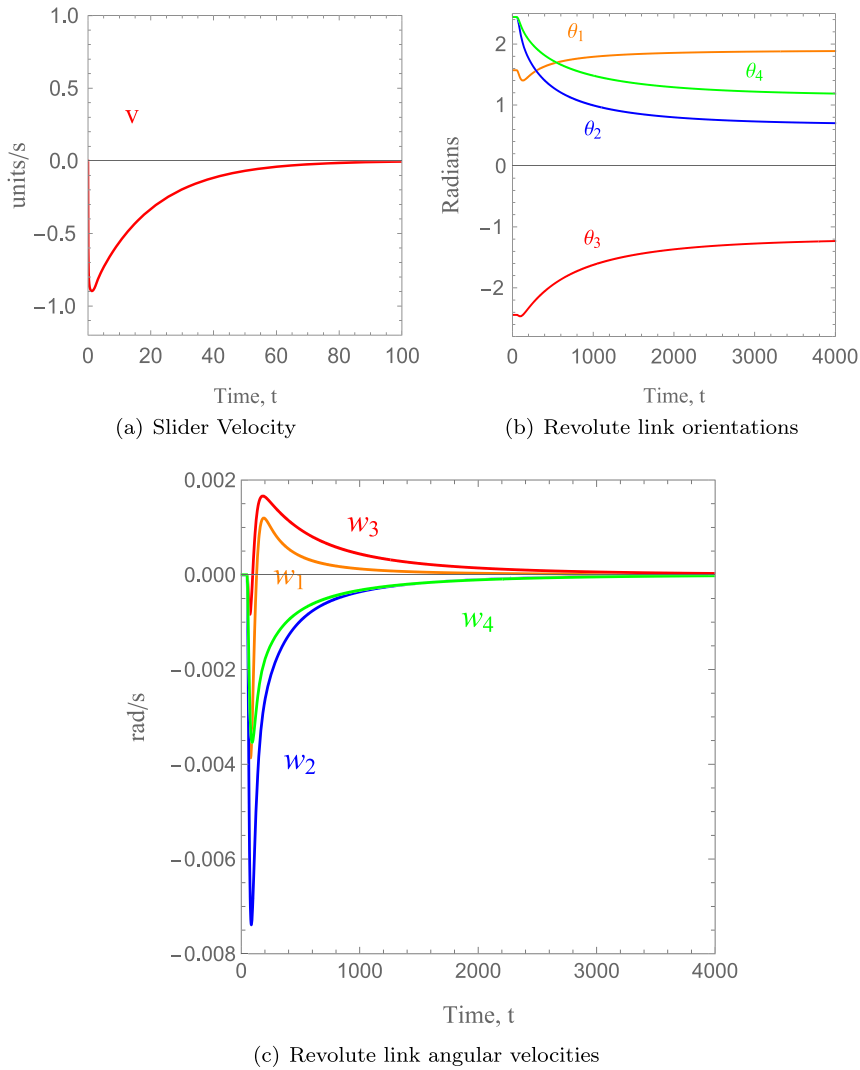(c) Revolute link angular velocities

Fig. 7. (a) Linear velocity of slider. (b) The revolute links orientations adhering to angular restrictions and limitations. (c) Angular velocities of the revolute links of the robotic arm.

Table 4
Numerical values of convergence parameters, initial states, and control parameters.

x-coordinate at the end of the rail	$r_l = 20$
Length of Slider	$2d = 4$
Coordinate of Slider Target	$(\eta, 0) = (17, 0)$
Number of revolute links	$n = 5$
Lengths of revolute links	$l_1 = l_2 = l_3 = l_4 = l_5 = 5.5$
Initial orientations of revolute links	$\theta_{1_0} = \frac{2\pi}{3}, \theta_{2_0} = -\frac{7\pi}{9}, \theta_{3_0} = \frac{7\pi}{9}, \theta_{4_0} = -\frac{7\pi}{9}$ and $\theta_{5_0} = \frac{7\pi}{9}$
Initial position of slider	$(x_{1_0}, 0) = (4, 0)$
End-Effector Target	$(a, b) = (27, 25)$
Obstacle avoidance parameter	$\gamma_1 = \gamma_2 = 0.002, \gamma_3 = \gamma_4 = \gamma_5 = \gamma_6 = \gamma_7 = \gamma_8 = 0.003$
Angular velocity restriction parameters of the revolute links	$\beta_1 = \beta_2 = \beta_3 = \beta_4 = \beta_5 = 0.005$
Slider convergence parameter	$\delta_1 = 14$
Revolute link angular velocity convergence parameters	$\delta_2 = \delta_3 = \delta_4 = \delta_5 = \delta_6 = 0.2$

(a) Initial positions, final positions and orientations

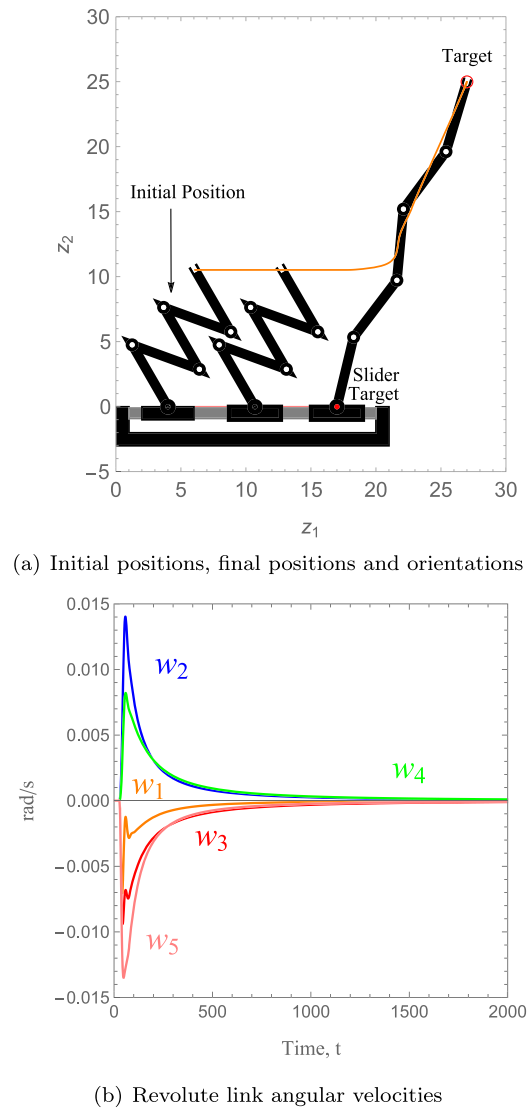(b) Revolute link angular velocities

Fig. 8. (a) Positions of the 5-link revolute robotic arm on the linear slider at times $t = 0, 9$, and 4000, respectively. The end-effector's trajectory is traced in orange. (b) Angular velocities of the revolute links of the robotic arm.

8. Discussion

This paper addresses MPC of an unanchored linear manipulator. The proposed system has higher flexibility as it can move easily along the rail to perform assigned tasks. Its increased mobility offers better use of space and has the ability to contribute towards high productivity when compared to the anchored manipulators presented in [13] and [18]. The linear manipulator system presented in this study is a modification of existing robotic arms due to its ability to reposition and navigate to distant targets, resulting from a change in work requirements. Furthermore, based on the users application, the generalized n-link revolute arm allows the user to select a definite number of links (n) while employing the same control laws.

The simulation results of Scenario 1, Scenario 2, and Scenario 3 show the effectiveness of the acceleration controllers and the proposed generalized version of the linear manipulator. As shown, the mobile slider and robotic arms perform designated tasks. The simulation results indicate that the proposed acceleration-based controllers are more feasible, effective, and facilitate a smooth motion than the trajectory tracking performance of the robotic arms with velocity-based controllers utilized in [56] and [30], which give rise to algorithm singularities and sharp changes in angular velocities resulting in erratic motion [31,32]. The response curves of the linear velocity of the slider (Fig. 4(d), Fig. 7(a)), and the angular velocities of the revolute links (Fig. 5(b), Fig. 7(c), Fig. 8(b)) indicate that the acceleration-based controllers designed in this research indicate good trajectory tracking performance of both the mobile slider and the revolute arm. Under the proposed controllers, it was observed that the slider and the end-effector successfully reached their targets, having a smooth and safe trajectory in all three scenarios. Moreover, the Lyapunov function's behavior indicates that the linear manipulator system had no difficulty in converging to its targets.

The unanchored mechanical system presented in this research is applicable to the industrial sectors such as aerospace and aviation, automotive, engineering, construction and building. Specifically, when the workspace is constrained, a mobile manipulator which can move in non-linear directions cannot facilitate the movement of an item from one station to another. Then, the proposed system can perform a double movement to facilitate motion with increased flexibility as the slider can move along the rail and enable the end-effector to achieve all configurations with increased reachability. For instance, the proposed system is applicable where consistency through process repeatability is required, and would be especially valued in the industrial production, manufacturing, factory automation, and assembly sectors. With an additional feature of a robotic arm mounted on a mobile slider operating along a rail, the linear manipulator addressed in this research possesses the ability to improve the quality of product and work environment by making industrial operations efficient and cost-effective for manufacturing companies [12].

9. Conclusion

The Lyapunov-based control scheme was successfully utilized to derive a new set of continuous time-invariant control laws of an unanchored linear manipulator comprising n-link robotic arm mounted on a mobile slider along a rail. The proposed acceleration controllers, governed by kinematic equations, facilitated feasible trajectories of the manipulator and ensured precise convergence of the system to the equilibrium state while satisfying all the constraints and singularities tagged on the system. From the authors' viewpoint, this is the first time that such continuous acceleration-based controllers have been developed for an n-link robotic arm linear manipulator system in the sense of Lyapunov.

This study is a theoretical exposition into the implementation of LbCS in solving the MPC problem of linear manipulators, whereby the authors have restricted themselves to demonstrating the capabilities of the derived acceleration-based control laws numerically, using computer simulations of interesting scenarios. The proposed linear manipulator provides dual advantage of mobility offered by the manipulator's mobile slider base and agility of the revolute arm end-effector, which offers several operational functionalities. Such a system combines the benefits of mobile platforms and robotic arms and reduces their individual drawbacks. It is viable for the industrial sector to include such controllers to develop autonomous linear manipulator systems that could perform tasks like material handling, pick and place, and assembly line applications. While the overall framework presented can be generalized to consider dynamics objectives and constraints, it has not been fully explored yet in this research. Dynamics, particularly how exerted forces and moments could fit into the framework of linear manipulators, will be considered as future work.

Declaration of competing interest

The authors declare no conflict of interest.

References

[1] A. Prasad, B. Sharma, J. Vanualailai, S.A. Kumar, Stabilizing controllers for landmark navigation of planar robots in an obstacle-ridden workspace, J. Adv. Transp. 2020 (6) (2020) 1–13.
[2] A. Gasparetto, L. Scalera, A brief history of industrial robotics in the 20th century, Adv. Hist. Stud. 8 (1) (2019) 24–35.
[3] B. Sharma, J. Vanualailai, S. Singh, Motion planning and posture control of multiple n-link doubly nonholonomic manipulators, Robotica 35 (1) (2017) 1–25.
[4] B. Sharma, J. Raj, J. Vanualailai, Navigation of carlike robots in an extended dynamic environment with swarm avoidance, Int. J. Robust Nonlinear Control 28 (2) (2018) 678–698.
[5] B. Sharma, S. Singh, J. Vanualailai, A. Prasad, Globally rigid formation of n-link doubly nonholonomic mobile manipulators, Robot. Auton. Syst. 105 (2018) 69–84.
[6] M. Nasrollahi, J. Ramezani, M. Sadraei, A FBWM-PROMETHEE approach for industrial robot selection, Heliyon 6 (5) (2020) e03859.
[7] M. Moghaddam, S.Y. Nof, Parallelism of pick-and-place operations by multi-gripper robotic arms, Robot. Comput.-Integr. Manuf. 42 (2016) 135–146.
[8] Y. Liu, X. Xin, Controllability and observability of an n-link planar robot with a single actuator having different actuator–sensor configurations, IEEE Trans. Autom. Control 61 (4) (2015) 1129–1134.
[9] A. Prasad, B. Sharma, S.A. Kumar, Strategic creation and placement of landmarks for robot navigation in a partially-known environment, in: 2020 IEEE Asia-Pacific Conference on Computer Science and Data Engineering (CSDE), IEEE, 2020, pp. 1–6.
[10] S. Makris, Cooperative manipulation-the case of dual arm robots, in: Cooperating Robots for Flexible Manufacturing, Springer, 2021, pp. 123–132.
[11] L. Gualtieri, E. Rauch, R. Vidoni, Emerging research fields in safety and ergonomics in industrial collaborative robotics: a systematic literature review, Robot. Comput.-Integr. Manuf. 67 (2021) 101998.
[12] H.A. Almurib, H.F. Al-Qrimli, N. Kumar, A review of application industrial robotic design, in: 2011 Ninth International Conference on ICT and Knowledge Engineering, IEEE, 2012, pp. 105–112.
[13] R. Chand, S.A. Kumar, R.P. Chand, Navigation of an n-link revolute robotic arm via hierarchal landmarks, in: 2021 3rd Novel Intelligent and Leading Emerging Sciences Conference (NILES), IEEE, 2021, pp. 188–192.
[14] R.L. Steinberg, B.A. Johnson, J.A. Cadeddu, Magnetic-assisted robotic surgery: initial case series of reduced-port robotic prostatectomy, J. Robot. Surg. 13 (4) (2019) 599–603.
[15] S.A. Kumar, J. Vanualailai, A. Prasad, Assistive technology: autonomous wheelchair in obstacle-ridden environment, PeerJ Comput. Sci. 7 (2021) e725.
[16] A.H. While, S. Marvin, M. Kovacic, Urban robotic experimentation: San Francisco, Tokyo and Dubai, Urban Stud. 58 (4) (2021) 769–786.
[17] D.L. Leistner, R.L. Steiner, Uber for seniors?: exploring transportation options for the future, Transp. Res. Rec. 2660 (1) (2017) 22–29.
[18] R. Chand, R.P. Chand, S.A. Kumar, Switch controllers of an n-link revolute manipulator with a prismatic end-effector for landmark navigation, PeerJ Comput. Sci. 8 (2022) e885.
[19] S.A. Kumar, J. Vanualailai, B. Sharma, A. Chaudhary, V. Kapadia, Emergent formations of a Lagrangian swarm of unmanned ground vehicles, in: 2016 14th International Conference on Control, Automation, Robotics and Vision (ICARCV), IEEE, 2016, pp. 1–6.
[20] A. Tringali, S. Cocuzza, Globally optimal inverse kinematics method for a redundant robot manipulator with linear and nonlinear constraints, Robotics 9 (3) (2020) 61.

[21] A. Tai, M. Chun, Y. Gan, M. Selamet, H. Lipson Para, A one-meter reach, two-kg payload, three-DoF open source robotic arm with customizable end effector, HardwareX 10 (2021) e00209.

[22] G. Caiza, C.A. Garcia, J.E. Naranjo, M.V. Garcia, Flexible robotic teleoperation architecture for intelligent oil fields, Heliyon 6 (4) (2020) e03833.

[23] S.A. Kumar, B. Sharma, J. Vanualailai, A. Prasad, Stable switched controllers for a swarm of UGVs for hierarchal landmark navigation, Swarm Evol. Comput. (2021) 100926.

[24] K. Chaudhary, G. Lal, A. Prasad, V. Chand, S. Sharma, A. Lal, Obstacle avoidance of a point-mass robot using feedforward neural network, in: 2021 3rd Novel Intelligent and Leading Emerging Sciences Conference (NILES), IEEE, 2021, pp. 210–215.

[25] V. Chand, A. Prasad, K. Chaudhary, B. Sharma, S. Chand, A face-off-classical and heuristic-based path planning approaches, in: 2020 IEEE Asia-Pacific Conference on Computer Science and Data Engineering (CSDE), IEEE, 2020, pp. 1–6.

[26] K. Chaudhary, A. Prasad, V. Chand, B. Sharma, ACO-kinematic: a hybrid first off the starting block, PeerJ Comput. Sci. 8 (2022) e905.

[27] R. Chand, M.R. Valluri, M.G. Khan, Digital signature scheme over lattices, in: 2021 25th International Conference on Circuits, Systems, Communications and Computers (CSCC), IEEE, 2021, pp. 71–78.

[28] Y. Pan, Y. Wu, H.K. Lam, Security-based fuzzy control for nonlinear networked control systems with DoS attacks via a resilient event-triggered scheme, IEEE Trans. Fuzzy Syst. (2022).

[29] Y. Pan, Q. Li, H. Liang, H.K. Lam, A novel mixed control approach for fuzzy systems via membership functions online learning policy, IEEE Trans. Fuzzy Syst. (2021).

[30] R.P. Chand, S.A. Kumar, R. Chand, R. Tamath, Lyapunov-based controllers of an *n*-link prismatic robot arm, in: 2021 IEEE Asia-Pacific Conference on Computer Science and Data Engineering (CSDE), IEEE, 2021, pp. 1–5.

[31] S.A. Kumar, J. Vanualailai, B. Sharma, A. Prasad, Velocity controllers for a swarm of unmanned aerial vehicles, J. Ind. Inf. Integr. 22 (2021) 100198.

[32] S.A. Kumar, J. Vanualailai, A. Prasad, Distributed velocity controllers of the individuals of emerging swarm clusters, in: 2020 IEEE Asia-Pacific Conference on Computer Science and Data Engineering (CSDE), IEEE, 2020, pp. 1–6.

[33] M.E. Moran, Evolution of robotic arms, J. Robot. Rurgery 1 (2) (2007) 103–111.

[34] H.Y. Chiu, Y.N. Kang, W.L. Wang, Y.S. Tong, S.W. Chang, T.H. Fong, P.L. Wei, Gender differences in the acquisition of suturing skills with the da vinci surgical system, J. Formos. Med. Assoc. 119 (1) (2020) 462–470.

[35] A. Gasparetto, L. Scalera, From the unimate to the delta robot: the early decades of industrial robotics, in: Explorations in the History and Heritage of Machines and Mechanisms, Springer, 2019, pp. 284–295.

[36] F.S. Miften, M. Diykh, S. Abdulla, S. Siuly, J.H. Green, R.C. Deo, A new framework for classification of multi-category hand grasps using EMG signals, Artif. Intell. Med. 112 (2021) 102005.

[37] A. Fayazi, N. Pariz, A. Karimpour, V. Feliu-Batle, S.H. HosseinNia, Adaptive sliding mode impedance control of single-link flexible manipulators interacting with the environment at an unknown intermediate point, Robotica 38 (9) (2020) 1642–1664.

[38] J. Wilson, M. Charest, R. Dubay, Non-linear model predictive control schemes with application on a 2-link vertical robot manipulator, Robot. Comput.-Integr. Manuf. 41 (2016) 23–30.

[39] G. Chaitanya, B.M. Krishna, Work space optimization of a RR planar manipulator using particle swarm optimization technique, Int. J. Eng. Sci. Technol. 9 (1) (2017) 46–54.

[40] H. Nakano, S. Sagara, R. Ambar, Resolved acceleration control (RAC) of dual-arm 3-link underwater robot: comparison of control performance between RAC method and computed torque method, in: 2018 International Conference on Information and Communication Technology Robotics (ICT-ROBOT), IEEE, 2018, pp. 1–4.

[41] J. Lee, J. Noh, S. Lee, W. Yang, A novel 4-DoF robotic link mechanism with e-CoSMo: kinematics based torque analysis, in: 2019 IEEE/RSJ International Conference on Intelligent Robots and Systems (IROS), IEEE, 2019, pp. 3577–3582.

[42] J. Iqbal, R.U. Islam, H. Khan, Modeling and analysis of a 6 DoF robotic arm manipulator, Can. J. Electr. Electron. Eng. 3 (6) (2012) 300–306.

[43] K. Asadi, R. Jain, Z. Qin, M. Sun, M. Noghabaei, J. Cole, K. Han, E. Lobaton, Vision-based obstacle removal system for autonomous ground vehicles using a robotic arm, in: Computing in Civil Engineering 2019: Data, Sensing, and Analytics, American Society of Civil Engineers, Reston, VA, 2019, pp. 328–335.

[44] A. De Luca, G. Oriolo, Trajectory planning and control for planar robots with passive last joint, Int. J. Robot. Res. 21 (5–6) (2002) 575–590.

[45] X. Xin, Linear strong structural controllability and observability of an *n*-link underactuated revolute planar robot with active intermediate joint or joints, Automatica 94 (2018) 436–442.

[46] A. Shafei, H. Mirzaeinejad, A novel recursive formulation for dynamic modeling and trajectory tracking control of multi-rigid-link robotic manipulators mounted on a mobile platform, Proc. Inst. Mech. Eng., Part I, J. Syst. Control Eng. 235 (7) (2021) 1204–1217.

[47] A. Prasad, B. Sharma, J. Vanualailai, S.A. Kumar, A geometric approach to target convergence and obstacle avoidance of a nonstandard tractor-trailer robot, Int. J. Robust Nonlinear Control 30 (13) (2020) 4924–4943.

[48] B. Sharma, J. Vanualailai, S. Singh, Lyapunov-based nonlinear controllers for obstacle avoidance with a planar *n*-link doubly nonholonomic manipulator, Robot. Auton. Syst. 60 (12) (2012) 1484–1497.

[49] A. Prasad, B. Sharma, J. Vanualailai, S.A. Kumar, Motion control of an articulated mobile manipulator in 3D using the Lyapunov-based control scheme, Int. J. Control (2021) 1–15.

[50] D. Rossi, E. Bertoloni, M. Fenaroli, F. Marciano, M. Alberti, Analytic hierarchy process to support the safety and ergonomic assessment of alternatives in manuable material handling, IFAC Proc. Vol. 46 (9) (2013) 525–530.

[51] R. Yu, Y. Li, C. Peng, R. Ye, Q. He, Role of 5G-powered remote robotic ultrasound during the COVID-19 outbreak: insights from two cases, Eur. Rev. Med. Pharmacol. Sci. 24 (14) (2020) 7796–7800.

[52] S.A. Kumar, K. Chand, L.I. Paea, I. Thakur, M. Vatikani, Herding predators using swarm intelligence, in: 2021 IEEE Asia-Pacific Conference on Computer Science and Data Engineering (CSDE), IEEE, 2021, pp. 1–6.

[53] S.A. Kumar, J. Vanualailai, B. Sharma, Lyapunov-based control for a swarm of planar nonholonomic vehicles, Math. Comput. Sci. 9 (4) (2015) 461–475.

[54] R.P. Chand, S.A. Kumar, R. Chand, LbCS navigation controllers of twining Lagrangian swarm individuals, in: 2021 3rd Novel Intelligent and Leading Emerging Sciences Conference (NILES), IEEE, 2021, pp. 183–187.

[55] S.A. Kumar, J. Vanualailai, A Lagrangian UAV swarm formation suitable for monitoring exclusive economic zone and for search and rescue, in: 2017 IEEE Conference on Control Technology and Applications (CCTA), IEEE, 2017, pp. 1874–1879.

[56] R. Chand, S.A. Kumar, R.P. Chand, S. Reddy, A car-like mobile manipulator with an *n*-link prismatic arm, in: 2021 IEEE Asia-Pacific Conference on Computer Science and Data Engineering (CSDE), IEEE, 2021, pp. 1–6.